Monte Carlo Simulation of Free-Standing Polymer Films near the Glass Transition Temperature

Tushar S. Jain and Juan J. de Pablo*

Department of Chemical Engineering, University of Wisconsin—Madison, Madison, Wisconsin 53706

Received October 19, 2001; Revised Manuscript Received January 2, 2002

ABSTRACT: Monte Carlo simulations have been applied to investigate the behavior of thin polymeric films near the glass transition. Free-standing films of both linear and cyclic polymeric chains have been considered in this work. In agreement with experiments, we find that the apparent glass transition temperature of free-standing films decreases with decreasing film thickness. We find that in free-standing films linear chains are no longer Gaussian but are considerably more compact. Near the glass transition temperature, the ring polymers show a slower bond relaxation than the linear chains; for a given film thickness, ring polymers exhibit a higher glass transition temperature than linear polymers of the same molecular weight. It is found that both linear and ring polymer thin films exhibit a fluidlike interfacial region where mobility is considerably higher than in the bulk of the film.

1. Introduction

Over the past few years, the glass transition of thin polymeric films has received considerable attention. Partly because thin films have a large surface area to volume ratio, thin films appear to exhibit thermodynamic, structural, and dynamic properties that are different from those of the bulk material. In particular, the glass transition temperature of thin free-standing polymer films (T_g) has been reported to change with film thickness and, in the case of supported films, also with the nature of substrate−polymer interactions.[1−5]

From a theoretical point of view, free-standing films are interesting because the two air−polymer interfaces are identical. Experimental data for these systems have revealed a number of intriguing features that remain largely unexplained. While this is still a matter of debate, most studies of free-standing films suggest that T_g decreases with decreasing film thickness. Two distinct molecular weight regimes have been identified in the case of free-standing polystyrene films.[2,6] For low to intermediate molecular weights ($M < 378\,000$), there is no clear dependence of T_g on M for films of a given thickness (h). Further, the depression of T_g with h is gradual and nonlinear. For high molecular weights, however ($M > 575\,000$), T_g can change considerably with M.

Various arguments have been proposed to explain the depression of T_g; many of these have been based on a higher concentration of chain ends[7−9] and depression of the density near the free interface.[10,11] It has also been proposed that the dynamics in thin films are dominated by a "sliding motion" mechanism which leads to the observed reduction of T_g.[12] Using scaling arguments, an expression for T_g has been derived that, in agreement with experiment, predicts a linear decrease of T_g with decreasing h for large molecular weights. The model assumes that the chains in the film are Gaussian and that the distribution of free volume for the motion of chain sites is also Gaussian. As pointed out by the author, however, the model is not entirely satisfactory in that its numerical predictions are not accurate, and it does not anticipate the disappearance of a molecular-weight dependence of T_g below a certain molecular weight.[12]

Experiments or simulations using ring molecules could provide useful insights into the dynamics of polymers in thin films. By eliminating the effects of chain ends, it would be possible to assess some of the assumptions of available theories. Available studies of ring polymers have focused on melt behavior in the bulk; lattice simulations suggest that ring chains exhibit a faster diffusion and orientation relaxation than linear chains.[13,14] This finding is somewhat counterintuitive, particularly in light of experiments which show that the diffusion coefficients of linear tracers in linear chain matrices are comparable to those of ring tracers in ring matrices.[15]

Recent simulations of polyethylene thin films have compared the dynamic behavior of linear and ring molecules at temperatures well above the glass transition.[11] After a careful analysis authors of that work concluded that the faster dynamics in the interfacial region that were observed for both linear and ring chains were due to a density depression at the interface. This finding suggests that chain ends are not responsible for the increase in mobility. However, the dynamics are known to change greatly in the vicinity of the glass transition temperature. One of the prevailing views of glasses in the bulk is that, near T_g, they consist of dynamic and collectively rearranging regions, characterized by a certain length scale.[16] Whether such dynamic heterogeneities exist or not in a thin film geometry and whether they are related to the chain ends or not is an open question. In this work, simulations of intermediate-length polymer chains are conducted to examine the dependence of T_g on thickness, the segmental mobility as a function of position in the film, and the dynamics of linear chains vis-á-vis those of ring molecules. We find that, near T_g, thin polymer films can be viewed as consisting of a fast, interfacial region and a slow, bulklike region. A dynamical analysis of these two regions suggests that both are relatively homogeneous. We also find that, in agreement with experimental data, the existence of this interfacial region leads to a depression of T_g with film thickness.

10.1021/ma011820e CCC: $22.00
Published on Web 02/16/2002

2. Simulation Details

2.1. Model and Simulation Methods. Polymer chains are represented by self-avoiding random walks on a cubic lattice of unit σ. The sites along the chains interact via a nearest-neighbor potential energy of magnitude $-\epsilon$. The chains considered in this work have 100 segments. All results are reported in reduced variables, i.e., temperature $T^* = kT/\epsilon$ and density $\phi = N\sigma^3/V$.

It is difficult to thermalize these systems at the low temperatures and high densities that characterize the glass transition. A wide variety of Monte Carlo moves are required to ensure adequate sampling of configuration space. Two general classes of moves, local and nonlocal, are employed in this work. Local moves involve the displacement of at most two sites during any trial Monte Carlo move. These moves are designed to mimic the actual motion of the chain at the local scale; we use kink-jump, crankshaft,[17] and end rotation moves. Trial moves are accepted or rejected on the basis of the standard Metropolis formulation,[18] subject to the constraints of bond connectivity and excluded volume. Local moves are used primarily to extract dynamic information from the simulations.

Nonlocal moves involve displacement of a large portion of the chain and are therefore more effective in equilibrating the system. Both reptation[19] and configurational bias (CB) moves are employed in this work. The latter moves are implemented in two different ways, referred to as "simple" and "rebridging". In simple CB moves[20,21] an end portion of the chain consisting of n sites is cut and regrown. For each growing site i, a total of k (for a self-avoiding chain on a cubic lattice $k = 5$) trial positions are considered, and one of these (l) is selected from the probability distribution

$$p_i^{(l)} = \frac{e^{-\beta U_i^{(l)}}}{\sum_{j=1}^{k} e^{-\beta U_i^{(j)}}} \tag{1}$$

where $U_i^{(j)}$ is the energy of interaction of site i in trial position j. The Rosenbluth factor of the chain is constructed from these probabilities according to

$$R_W^F = \prod_n \sum_{j=1}^{k} e^{-\beta U_i^{(j)}} \tag{2}$$

Trial moves are accepted with probability

$$P_{\text{acc}}(o \rightarrow n) = \min\left[1, \frac{R_W^F}{R_W^R}\right] \tag{3}$$

where R_W^R is the Rosenbluth factor of the chain in its original configuration. Simple CB moves are effective for equilibration of chains of small and intermediate length. For longer molecules, it is advantageous to use rebridging CB moves.[22] In this case, a part of the chain consisting of n sites is cut starting from site s of the chain. These sites are regrown with an energy bias (as in simple configurational bias) and an additional topological bias that preserves chain connectivity. The topological bias takes the form of the number of possible random walks from the current site i to site $s + n$. The probability distribution[22] then becomes

$$p_i^{(l)} = \frac{N^{(l)}(i, s+n) e^{-\beta U_i^{(l)}}}{\sum_{j=1}^{k} N^{(j)}(i, s+n) e^{-\beta U_i^{(j)}}} \tag{4}$$

where $N^{(j)}(i, s + n)$ is the number of random walks from site i in position j to site $s + n$. The modified Rosenbluth factor and the random-walk weight for the chain are constructed according to

$$R_W^F = \prod_n \sum_{j=1}^{k} N^{(j)}(i, s+n) e^{-\beta U_i^{(j)}} \tag{5}$$

$$G_{RW}^F = \prod_n N^{(l)}(i, s+n) \tag{6}$$

The acceptance criteria for a trial move reduce to

$$P_{\text{acc}}(o \rightarrow n) = \min\left[1, \frac{R_W^F G_{RW}^R}{R_W^R G_{RW}^F}\right] \tag{7}$$

where R_W^R and G_{RW}^R are the Rosenbluth weight and the random-walk weight for the reverse move. It should be noted that in the case of ring chains this type of move will not preserve the unconcatenated nature of the chains. If one were to start from an initial configuration consisting of unconcatenated rings, and only local moves were used, the unconcatenated nature would be preserved throughout the simulation. However, to equilibrate the systems faster in the vicinity of the glass transition, we have chosen to employ bridging moves for the ring chains.

Near the glass transition, the approximate acceptance rates for the various moves employed in this work are 15% for reptation, 3% for local moves, and 50% for the CBMC moves. It should be noted that for the CBMC moves the abnormally high acceptance rate arises from the new configurations retracing the path of the old configuration. For the part of the study that involved calculating the dynamical properties of the chains, only local moves were employed. This approach has been used before to extract dynamic information from Monte Carlo studies[23−25] on a coarse-grained lattice. An attempted displacement for every occupied site, i.e., a Monte Carlo step, can be assigned a time step τ in real time. The quantity τ is system size independent, because it is defined in terms of time needed to attempt a displacement for every occupied site in the system. The number of sites moving in a given amount of time is proportional to the number of occupied sites in the system. The time correlation functions can then be plotted as a function of the number of attempted Monte Carlo steps, N_{mcs}, or in terms of time t ($t = \tau N_{\text{mcs}}$). In our simulations, configurations were mostly saved at regular intervals for subsequent analysis.

Figure 1 shows a schematic representation of the film and the coordinate system employed in this work. The starting point for the simulations was the spontaneous formation of a thick, free-standing film. The initial temperature was $T^* = 2.2$, and the initial density in the bulk of the film was $\phi = 0.85$. The surface area of the film was $125\sigma^2$. Each simulation was run until the system was well-equilibrated. We generated four different initial configurations containing a different number of chains ($N_c = 147$, 125, 94, and 81) by removing

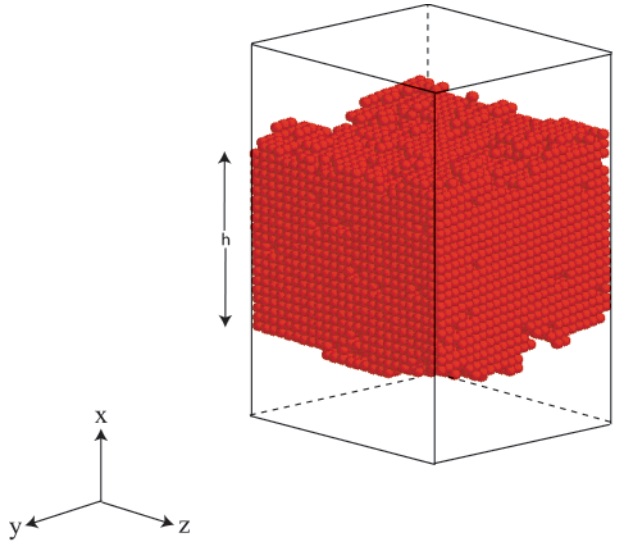

Figure 1. Schematic representation of the free-standing film.

the appropriate number of chains from the thickest film considered here. For a given film, the temperature was lowered in a stepwise manner. The final, fully relaxed configuration for a given temperature was subsequently taken as the starting point for the next run at a slightly lower temperature. At each temperature, the displacement of the center of mass of the chains ($g_1(t)$) and the site displacement in the center of mass coordinates ($g_2(t)$) were monitored. The simulations were run long enough to ensure that $g_1(t)$ was several radii of gyration and that $g_2(t)$ was constant. An apparent glass transition temperature was estimated by measuring the thickness of a given film as a function of temperature. The point at which the slope of the thickness vs temperature graph changes was identified with T_g.

All the simulations of *dynamic* properties were carried out on films of thickness ≈20, at $T^* = 1.1$ (near the estimated glass transition temperature of the film). The number of chains in the simulation (N_c) was 125 for both linear and ring polymers.

2.2. Properties. The film thickness was evaluated by calculating the center of mass of the film for every saved configuration; the "bulk" density was determined from the mean density in the region of the film near the center of mass. The film thickness was calculated by counting the number of lattice $y-z$ planes in the film having density greater than half the "bulk" density. The apparent glass transition temperature for the linear chains was identified with the change of the slope of the h vs T^* curve. For $h \approx 20$, T^*_g was estimated to be 1.02 for the linear chains and 1.1 for the ring chains.

We examined the radius of gyration, the orientation of the chains, the distribution of chain centers of mass, and the concentration of chain ends, all as a function of position in the film. The film was divided into interfacial and bulk regions; static and dynamic properties were calculated separately for these two regions.

The structure factor[26] for the chains was calculated for the film as a whole and for the interfacial and bulk regions. It is defined as

$$S_{sc}(k) = \frac{1}{L}\sum_{m=1}^{L}\sum_{n=1}^{L}\langle e^{i\vec{k}\cdot(\vec{r}_m-\vec{r}_n)}\rangle \qquad (8)$$

where $\vec{r}_m$ and $\vec{r}_n$ are site vectors, $\vec{k}$ is the scattering vector, and the brackets denote an average over the number of chains, states in the ensemble, and orientations of $\vec{k}$ in space.

A bond orientation autocorrelation function was defined to measure local dynamics according to

$$b(t) = \frac{\langle \vec{B}(t)\cdot\vec{B}(0)\rangle}{\langle \vec{B}(0)\cdot\vec{B}(0)\rangle} \qquad (9)$$

where $\vec{B}(t)$ is a bond vector at time t. The bond autocorrelation functions investigated here include the overall bond autocorrelation function, the bond autocorrelation function based on position of the site along the chain (only for linear chains), and the bond autocorrelation function based on position of the sites in the film. The latter correlation is particularly relevant in that some of the chains are not strictly confined to either the interface or the bulk, but have sites in both regions, as one can observe from the chain site distribution function (Figure 5). We also calculated the incoherent scattering function for the system. This function measures the displacements of a monomer with time; it is defined as[27]

$$\Phi^s_k(t) = \frac{1}{N_c L}\sum_{m=1}^{N_c L}\langle e^{i\vec{k}\cdot(\vec{r}_m(t)-\vec{r}_m(0))}\rangle \qquad (10)$$

where the coordinates $\vec{r}_m(t)$ and $\vec{r}_m(0)$ are evaluated at times t and 0, respectively. In the present work, the magnitude of k was set at 2π. To study the positional correlation between "fast" moving sites, a plot was constructed of the probability of a displacement at different times during the simulation. A discrete analysis was performed by considering two sets of sites, namely those having displacements equal to or greater than twice the average displacement of all sites and those having a displacement equal to or greater than three times the average displacement. Sites with displacements 3 times or more than the average were found to be confined to the interfacial region (for both linear and ring polymers) over the entire duration of the simulation. The distribution of sites having displacements greater than twice the average extends into the bulk region of the film. The average size of these dynamical inhomogeneities (fast moving sites found together) was ∼4 in the case of linear chains and ∼3 in the case of ring chains. Furthermore, in the case of linear polymers, these sites were mostly but not always the terminal sites of the chains. We did not find any apparent correlation between the positions of these clusters in the film as found by other investigators.[28]

The center-of-mass diffusion coefficient (D) was calculated for the film of linear chains as a function of temperature. Only the y and z components of the mean-square displacement (of the center of mass) were used to calculate D. For several temperatures, the individual diffusion coefficients were also calculated for the interfacial and the bulk regions of the film. We emphasize that only local moves were used to calculate dynamic properties.

3. Results

3.1. Equilibrium Properties. The thickness of the films as a function of temperature is shown in Figure 2 for linear and ring polymer films of final thickness $h =$ 20 below the apparent glass transition. From this figure, the value of T^*_g was estimated to be 1.02 for linear

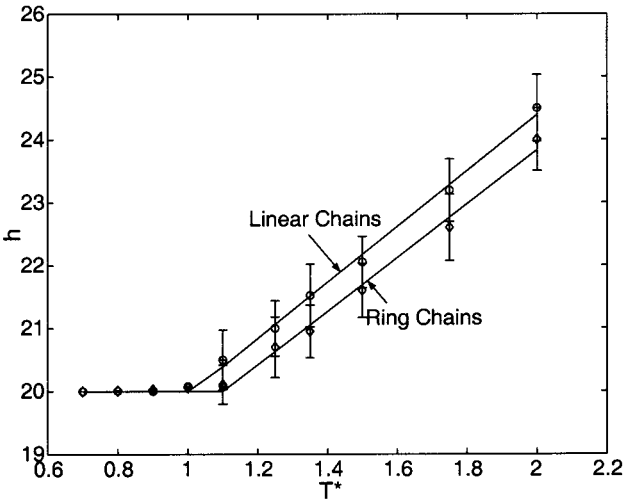

Figure 2. Film thickness h as a function of reduced temperature T^*.

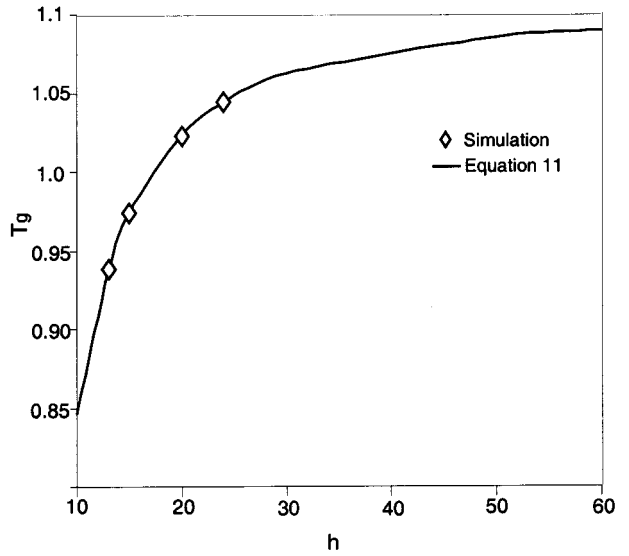

Figure 3. Glass transition temperature as a function of film thickness for linear chains.

chains and 1.1 for ring chains. Figure 3 shows a plot of T_g vs h for linear chains. The data were fit to the functional form[1]

$$T^*_g = T^*_{gb}\left[1 - \left(\frac{a}{h}\right)^{\delta}\right] \qquad (11)$$

where T^*_{gb} is the bulk glass transition temperature; a and δ are constants. The best fit of simulation results was achieved with $T^*_{gb} = 1.1$, $a = 4.24$, and $\delta = 1.71$. The experimental data for free-standing films of polystyrene (PS) ($T_{gb} = 374$ K) in the low-M_w regime is fit by $a = 7.8$ nm and $\delta = 1.8$.[6] If we take the Kuhn length of PS to be ≈1.8 nm, then the value of $\sigma \approx 1.5$ nm, and this leads to $a = 6.2$ nm, which is a reasonable agreement between simulation results and experimental data.

The density profile for the linear and ring chains is shown in Figure 4. The chains form a continuous film, and as expected, the density tapers off to zero near the interface. The highest densities in both films are $\phi \sim 0.97$. We therefore do not expect the difference in dynamic behavior (discussed later in the paper) to be caused by a free-volume difference. An important distinction between the density profiles for rings and linear chains is that for the former the film is flatter (i.e., they exhibit a sharper decay to zero at the interface). This is due to the greater ability of ring chains to pack more efficiently, which in turn arises from the topological constraint to form a closed path. Linear chains have more conformations accessible to them (due to the free ends), and this enables them to offset the enthalpic penalty in the interfacial region associated with having fewer contacts with neighboring polymer sites.

An interfacial and a bulk region were defined by dividing the film into five sections of equal thickness. The distribution of sites as a function of position was calculated on the basis of the position of the center of mass of the chains in any one of these sections (see Figure 5). The bulk region was defined as the portion of the film consisting of lattice sites between peaks 2 and 4. Chains having their center of mass in this region were labeled as "bulk" chains. Figure 5 shows that the peaks for the interfacial regions are higher than those for the bulk. This implies that chains at the interface are localized near their center of mass to a higher extent than bulk chains. As shown in Figure 6, the concentration of chain ends is higher at the interfaces. The absolute chain end density was normalized by the site density in each yz plane. This is consistent with previous work, both theoretical[8] and experimental,[7,9] and it is due to the fact that end sites are bonded to just one neighbor and therefore have more freedom to move and access a greater number of conformations than sites that are bonded to two polymer segments. This higher gain in entropy offsets the enthalpic penalty associated with the low-density interfacial region.

Figure 7 shows the distribution of $\langle R_g^2\rangle^{1/2}$ as a function of position in the film. It can be seen that linear chains are significantly smaller near the interface than in the bulk; the vacuum above the film behaves as a poor solvent, and the attraction between chain sites dominates their conformation. Ring chains have a smaller $\langle R_g^2\rangle^{1/2}$ than linear chains; unfortunately, the variation in $\langle R_g^2\rangle^{1/2}$ from the interface to the bulk is not as clear for ring chains as it is for linear chains.

Figure 8 shows the probability distribution of ϕ and θ, which are the angles made by the longest ellipsoidal axis of a chain with the x and y axes, respectively. (Each chain is reduced to an equivalent ellipsoid following literature procedures.[29]) The moment of inertia tensor is calculated for the chains; its eigenvalues give the length of the semiaxes, and its eigenvectors give the directions of these axes. Linear chains near the interface are considerably more planar and lie in the plane; chains in the bulk region are oriented at random. The corresponding results for ring chains (not shown) are similar.

Figure 9 shows the structure factor of linear chains in the interfacial and bulk regions. In the limit of long chains and $kR_g \gg 1$, the decay goes as $k^{-1/\nu}$ where $\nu = {}^1/_2$ for a Gaussian chain in the melt. Polymers in the glassy state retain their bulk Gaussian nature.[30] In contrast, we find that $\nu = 0.455 \pm 0.005$ near the interface and $\nu = 0.472 \pm 0.005$ in the "bulk" of the film. The chains are non-Gaussian throughout the film, and the deviations are larger in the interfacial region. However, on examining the individual components of the radius of gyration of the chains (not shown), we found that there was no significant change in the radius

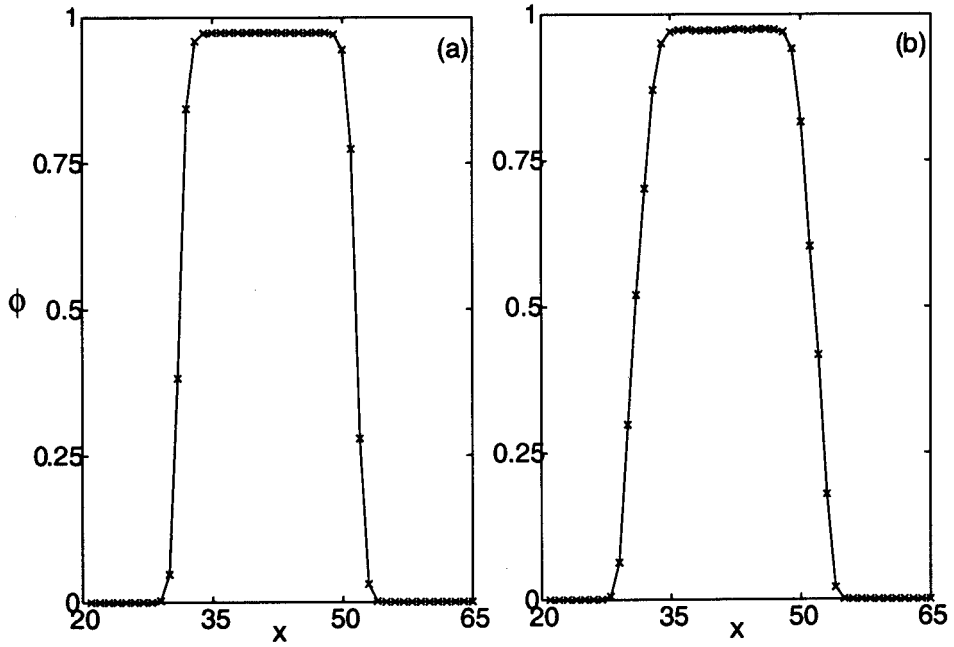

Figure 4. Density profile of the free-standing film for (a) ring chains and (b) linear chains.

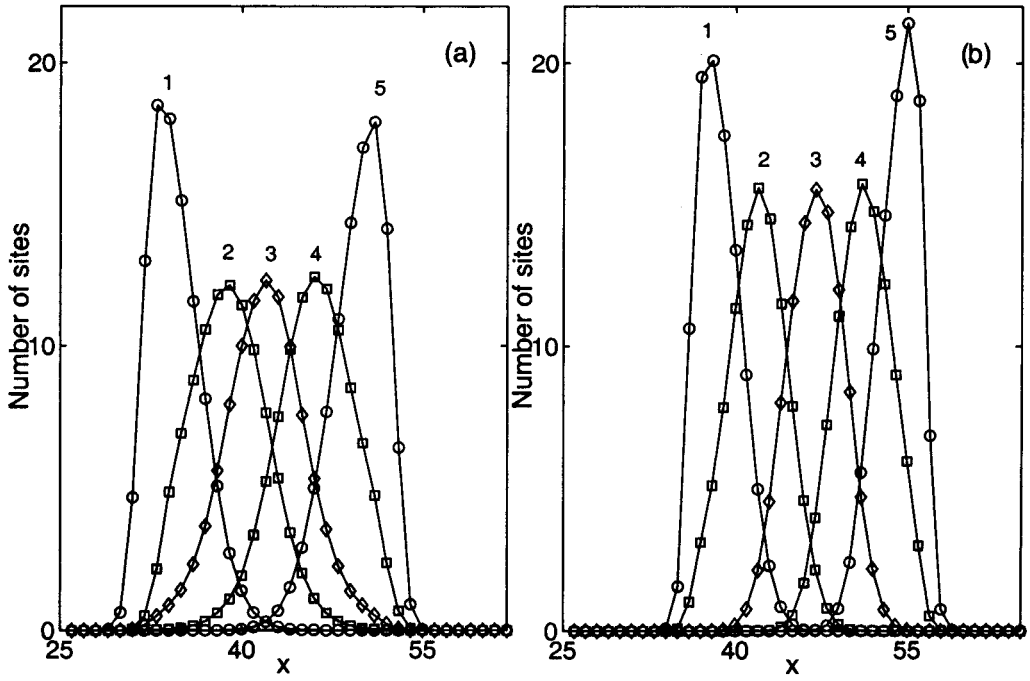

Figure 5. Average distribution of chain sites as a function of position in the film for (a) linear chains and (b) ring chains.

of gyration along the y and z directions (in the plane normal to the direction of confinement) as a function of position in the film. This agrees with the recent results obtained by Jones et al.[31] where they found that the chain dimensions in thin films were not perturbed in the directions parallel to the confinement direction. However, the films in these experiments were not free-standing but confined between two identical surfaces.

The structure factors for the ring chains in the interfacial region and bulk regions are shown in Figure 10. The value of the exponent for the chains in the bulk region of the film is $\nu = 0.392 \pm 0.006$. Literature results from melt simulations indicate that $\nu = 0.39$.[14] For interfacial chains, the structure factor shows two distinct slopes. At larger length scales, the exponent is $\nu = 0.385 \pm 0.006$; at smaller length scales it is $\nu = 0.435 \pm 0.004$. Because of the low density near the interface, the repulsive excluded-volume interaction is not offset by attraction from other neighboring sites to the same extent as in the bulk of the film. This results in the chains being more expanded on the local scale than the chains in the bulk. Therefore, at the shorter length scale the exponent is higher than that for the melt condition. At the larger length scale, as the chain probes the inner dense region of the film, this excluded-volume interaction is screened out and the exponent is the same as for the bulk ring chains.

Figure 11 shows the center-of-mass distribution as a function of position in the film. An oscillatory profile can be seen in both the cases indicating a layering of the chains in the films. Two distinct peaks are observed in the case of linear chains which result from the chains

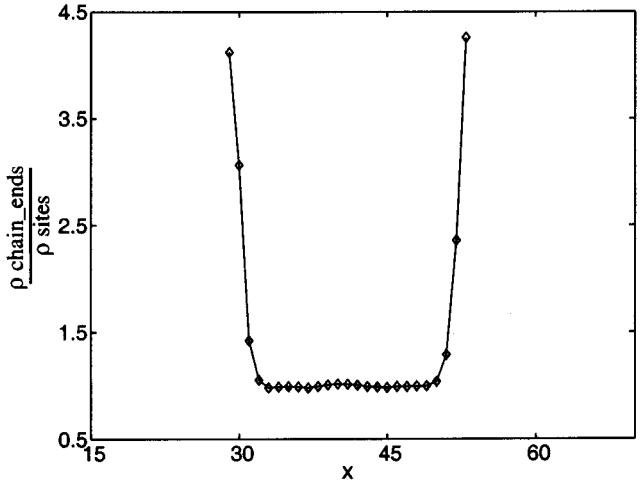

Figure 6. Relative chain end concentration ($\rho_{\text{chain ends}}/\rho_{\text{sites}}$) in the film, normalized with respect to bulk of the film.

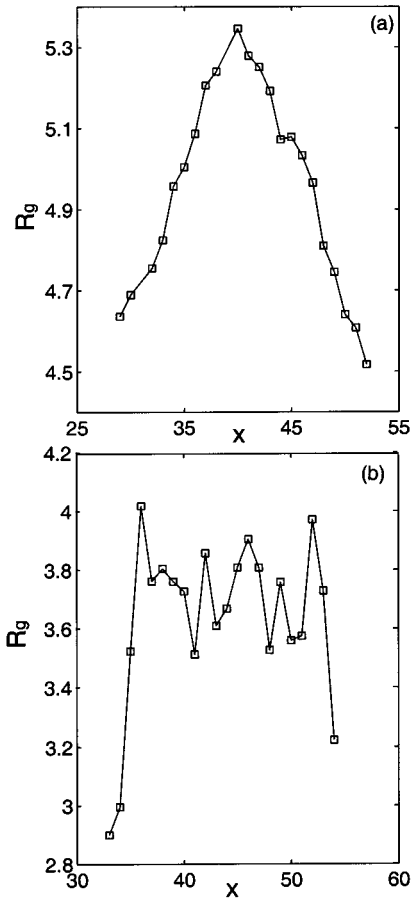

Figure 7. Radius of gyration as a function of position in the film for (a) linear chains and (b) ring chains.

being flattened at the interface compared to the bulk. Three peaks can be seen in the case of ring chains, which is due to the fact that they are smaller in size than the linear chains, and therefore, more layers of the chains can fit in the film for a given film thickness (≈20 in this case). The peaks at the interface are higher, again indicating that the chains are more flattened at the interface than in the bulk. Mattice et al.[11] observed similar profiles for the chain centers of mass in the case of polyethylene chains at meltlike temperatures for both rings and linear chains.

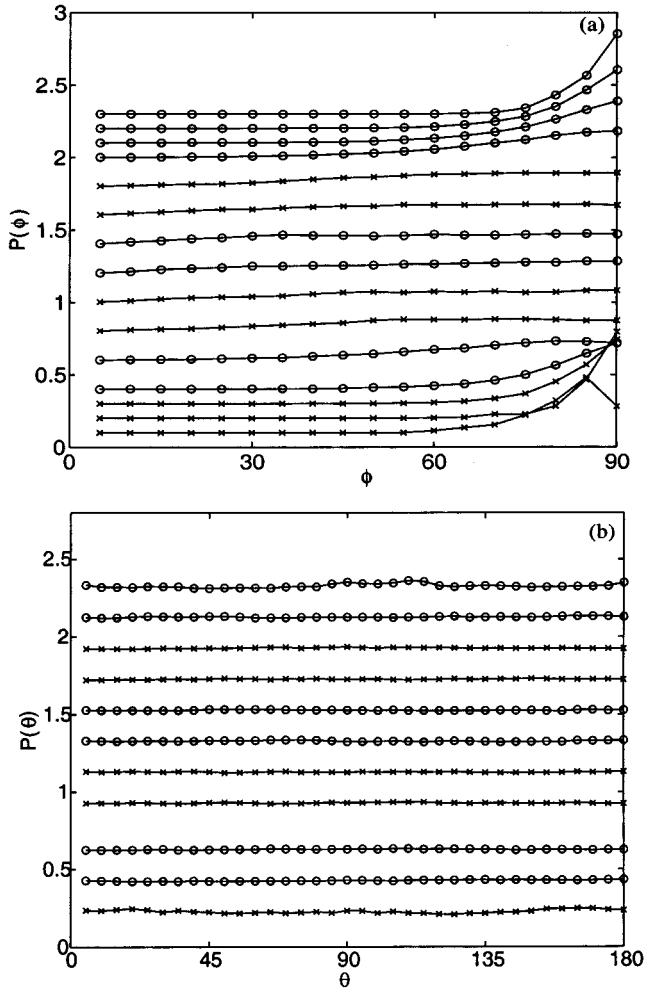

Figure 8. Probability distribution as a function of position in the film for angle made by the largest ellipsoidal axis of the chain with (a) the *x*-axis (ϕ) and (b) the *y*-axis (θ). The successive probability distributions are vertically offset by 0.1 for clarity.

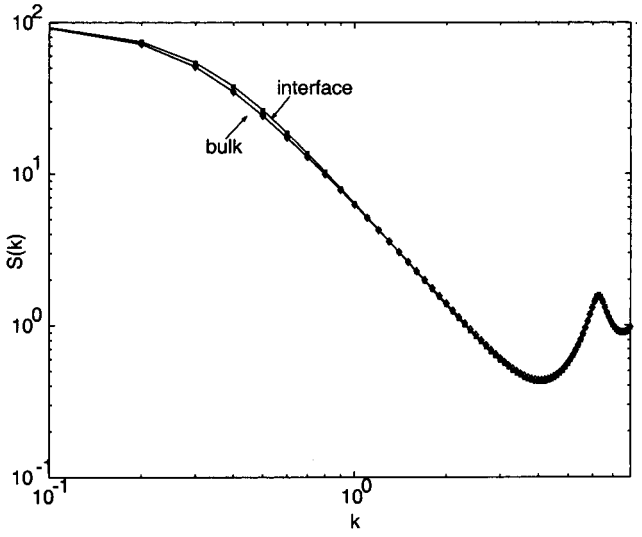

Figure 9. Structure factor for the bulk and interfacial linear chains.

3.2. Dynamic Properties. Figure 12 shows the bond autocorrelation function for linear chains as a function of position along the chain. Bonds at the ends of a linear chain decay faster than bonds toward the middle of the molecule, but the difference in decay disappears after

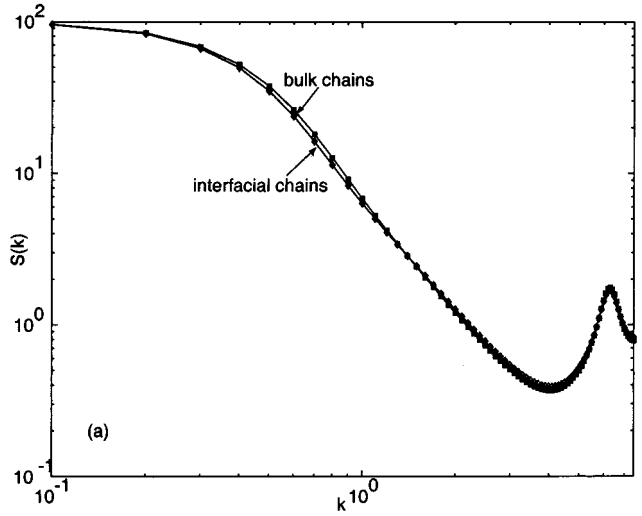

Figure 10. Structure factor for bulk and interfacial ring chains.

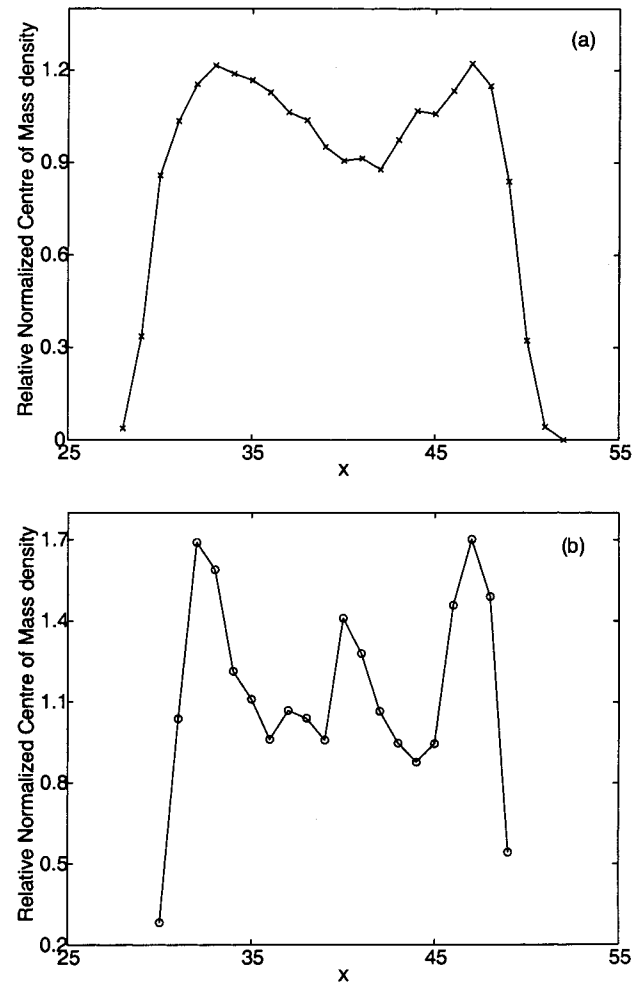

Figure 11. Chain center-of-mass density normalized with respect to bulk for (a) linear chains and (b) ring chains.

about five sites from the end. The average bond autocorrelation for the ring chains is also shown.

As one can see from the segmental distribution probabilities, several chains have sites in both the interfacial and bulk regions. To investigate segmental mobility as a function of position in the film, several bond autocorrelation functions are calculated according to the following procedure:

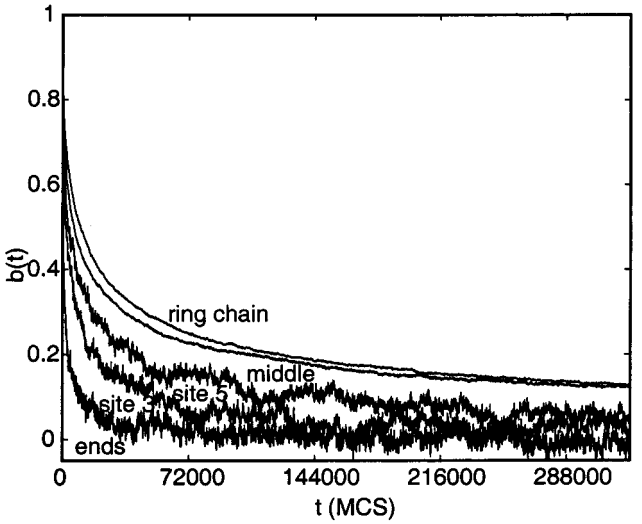

Figure 12. Bond autocorrelation function for ring chains and for linear chains as a function of position of site along the chain.

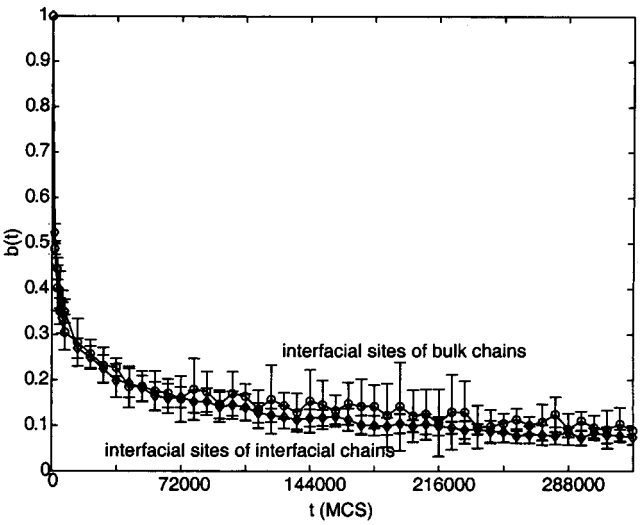

Figure 13. Bond autocorrelation function for the interfacial sites of linear chains.

(i) The simulation was divided into four blocks of equal number of attempted Monte Carlo steps. In each block, the chains that were *always* in the interfacial region or *always* in the bulk region for an entire block were used for further calculation.

(ii) The next part involved isolating those sites that belonged to the selected chains and that, in *addition*, were always in either the interfacial or bulk region for a given block of the simulation. Note that, by construction, these selected sites will be those with lower mobility perpendicular to the plane of the film.

(iii) The sites selected above were used to calculate the bond autocorrelation functions shown in Figures 13−16.

Figures 13 and 14 show that the orientation of bulk-chain bonds in the interfacial region decays slower than that of interfacial-chain bonds in the interfacial region. However, as can be seen from Figures 15 and 16, the orientation of interfacial-chain bonds in the bulk portion of the film decays slower than that of bulk-chain bonds in the bulk region. Note, however, that the errors associated with correlation functions for sites away from the region where the larger part of the chain resides

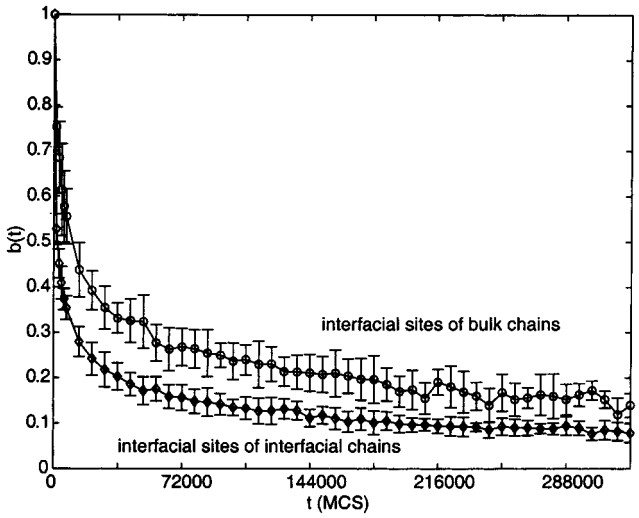

Figure 14. Bond autocorrelation function for the interfacial sites of ring chains.

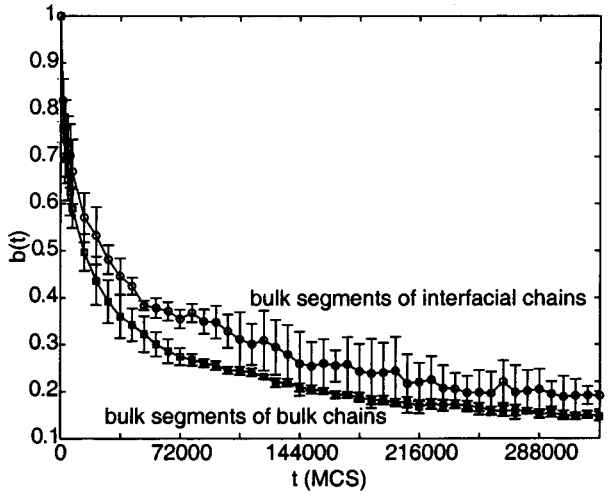

Figure 15. Bond autocorrelation function for the bulk sites of linear chains.

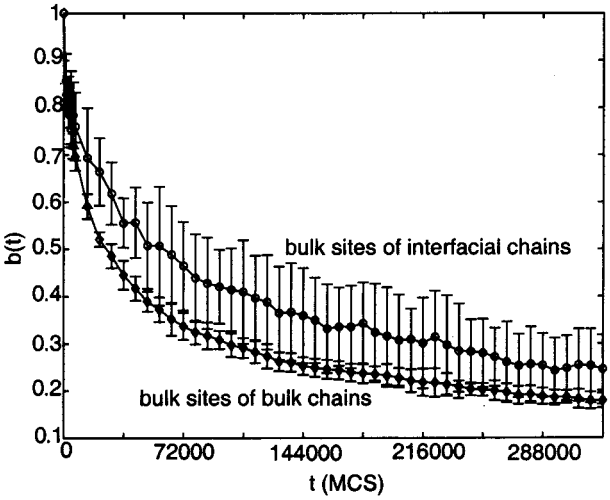

Figure 16. Bond autocorrelation function for the bulk sites of ring chains.

are greater, because these sites are fewer in number and the statistics are poorer. In general, one can conclude from the correlation functions that the relaxation of ring chains is slower than that of linear chains in all parts of the film. This conclusion is further

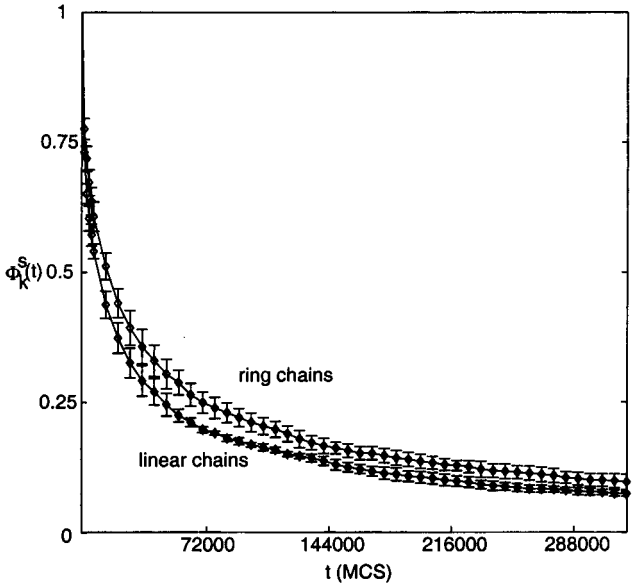

Figure 17. Incoherent scattering function ($\Phi_k^s(t)$) for linear and ring chains.

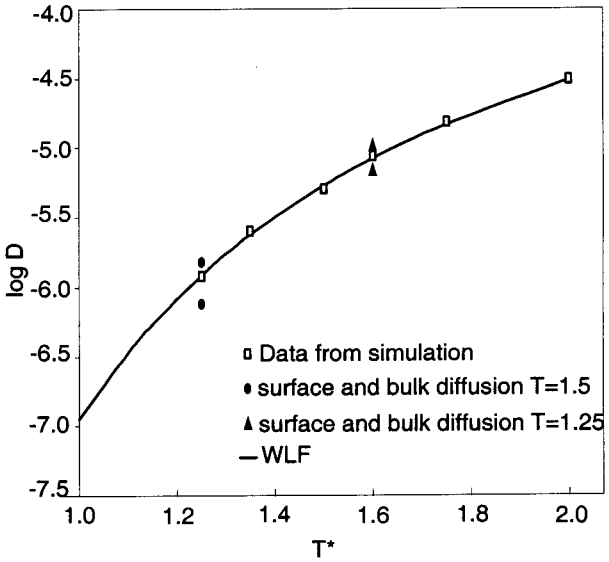

Figure 18. Diffusion constant D as a function of reduced temperature T^*.

corroborated by Figure 17, which shows the incoherent scattering function for linear and ring polymers. It can be seen that the fluctuations in position in linear chains are greater at the length scale of a bond ($k = 2\pi$) than in ring chains.

The center-of-mass diffusion coefficients D are shown in Figure 18 for the $h = 20$ film of linear chains as a function of temperature. We have also determined separate diffusion constants for the surface layer and the bulk of the film at two different temperatures. We can see that the difference between these two contributions from the global D increases with decreasing temperatures. It is important to point out, however, that it is difficult to get a statistically sound estimate of the individual diffusion constants, as a large number of the chains do not remain in one of the regions throughout the entire course of the calculation. The values reported in Figure 18 as a function of position in the film are our best estimates. One can conclude from that figure that the motion of the surface layer becomes increas-

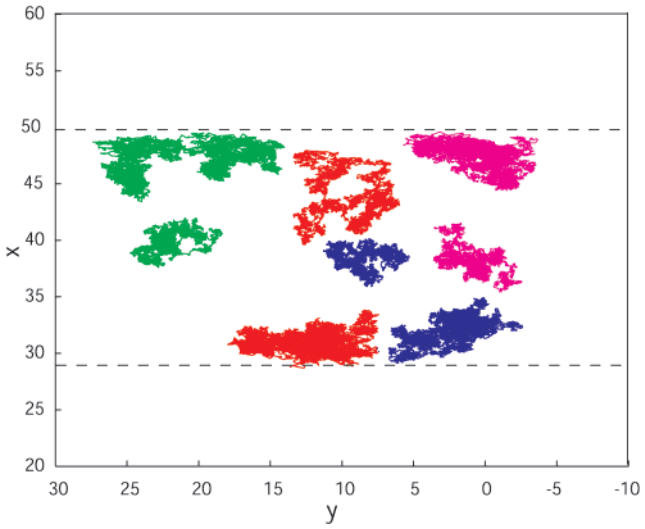

Figure 19. Typical trajectories for the chain centers of mass at $T^* = 1.25$.

ingly important as the glass transition is approached and that it dominates mobility in the film. This can also be seen in Figure 19, which shows the typical trajectories of the centers of mass of the chains at $T^* = 1.25$, during the same interval of time. As one can see, the displacement of the chains in the interfacial region is greater than that for the chains in the bulk. The data for D was fit to the Williams−Landel−Ferry (WLF) form

$$\log\left[\frac{D(T)}{D(T_g)}\right] = \frac{C_1(T - T_g)}{C_2 + T - T_g} \qquad (12)$$

where C_1 and C_2 are two constants which depend on polymer relaxation and glass fragility, respectively.[32] The diffusion constant for the linear chains at T_g was set at $10^{-17}\sigma^2\tau^{-1}$.[32] The best fit values for these parameters are $C_1 = 14.51$ and $C_2 = 0.254$. On the basis of relaxation time and viscosity data for polymers, it has been argued that if C_1 is in the range from 16 to 17, and the fragility (f) can be calculated from $f = 1 - C_2/T_g$. Though the C_1 value for our system is slightly below this range, we still use this equation for f to provide an approximate measure of the fragility of our system. We find $f = 0.40$. This value is consistent with previous simulations of free-standing films performed by Torres et al.[4] for an off-lattice model using shorter chains. The glass transition temperature predicted by the WLF fit is lower than that obtained from the thickness plot, which points toward the role of higher surface diffusion for thin films. (The diffusion constants for ring chains are not presented because some of the molecules are concatenated.)

4. Discussion

From our simulations, we have seen that linear chains in thin films are not Gaussian. However, the chain dimensions are largely unperturbed parallel to the plane of confinement, which is in qualitative agreement with experiments on films confined between identical surfaces.[31] The dimensions are more compact in the direction of confinement for a major portion of the film, and we feel that this contributes to the overall non-Gaussian nature of the polymer coil. In the recently proposed "sliding" motion,[12] it is postulated that there is an additional mode of motion in the thin film that arises due to motion in the loops of the chains extending from the interface into the bulk of the film. As the chains are more compact in the interfacial region, we feel that the penetration of the loops from the interfacial region into the bulk of the film would be lesser than that predicted by using a Gaussian approximation. Also, from our analysis of the positional correlation we did not find a clear evidence of large-scale collective sliding motion in the bulk of the film at the thicknesses considered here.

Our simulations support the view that thin polymer films near T_g consist of a "semifluid" interfacial layer and a bulk region. The glass transition temperature of the films was found to decrease with film thickness, with a dependence consistent with experiments.[1] The chain-end concentration is significantly higher than in the bulk in the outermost regions of the interface; this supports the view of Mattice et al. that chain ends only contribute to an increase in mobility in the outer regions of the interface, where mobility is high anyway. However, as discussed before, we found that the dynamical inhomogeneities in the bulk of the film were largely near the chain ends for the linear chains.

Our analysis indicates that segmental mobility is a function of position of the chain in the film (bulk vs interfacial regions), position of a site in the film, and position of a site along the chain. When the center of mass of a molecule is well into the bulk region, segments belonging to that molecule but lying in the interfacial region tend to move faster than the rest of the molecule. These segments, however, are somewhat slower than most other polymer sites in the interfacial region. The incoherent scattering function decayed faster for linear chains than for rings, showing a faster segmental motion in the case of linear chains. This is also borne out by the lower glass transition temperature for linear chains compared to that for ring chains.

The value of fragility calculated from the WLF fit is 0.4 whereas the value for a typical polymer melt is 0.8. Furthermore, the value of $C_1 = 14.5$ is somewhat lower than the typical value of 16−17 for most polymers in the bulk. These findings are consistent with those of previous simulations of much shorter chains.[4] Free interfaces have the effect of lowering the fragility of thin-film polymer glasses and that of accelerating the relaxation of the polymer film.

Acknowledgment. This work is supported by the Division of Chemical Sciences, Office of Basic Energy Sciences, Office of Science, and the United States Department of Energy (DE-FG02-99ER14961). Support from the Semiconductor Research Corporation is also acknowledged.

References and Notes

(1) Keddie, J. L.; Jones, R. A. L.; Cory, R. A. *Europhys. Lett.* **1994**, *27*, 59−64.
(2) Dalnoki-Veress, E.; Forrest, J. A.; Murray, C.; Gigault, C.; Dutcher, J. R. *Phys. Rev. E*, in press.
(3) Fryer, D. S.; Nealey, P. F.; de Pablo, J. J. *Macromolecules* **2000**, *33*, 6439−6447.
(4) Torres, J. A.; Nealey, P. F.; de Pablo, J. J. *Phys. Rev. Lett.* **2000**, *85*, 3221−3224.
(5) Fryer, D. S.; Peters, R. D.; Kim, E. J.; Tomaszewski, J. E.; de Pablo, J. J.; Nealey, P. F.; White, C. C.; Wu, W. L. *Macromolecules* **2001**, *34*, 5627−5634.
(6) Mattsson, J.; Forrest, J. A.; Börjesson, L. *Phys. Rev. E* **2000**, *62*, 5187−5200.
(7) Kajiyama, T.; Tanaka, K.; Takahora, A. *Macromolecules* **1997**, *30*, 280−285.

(8) Mayes, A. M. *Macromolecules* **1994**, *27*, 3114−3115.
(9) Zhao, W.; Zhao, X.; Rafailovich, M. H.; Sokolov, J.; Composto, R. J.; Omith, J. J.; Dozier, W. D.; Mansfield, J.; Russell, T. P. *Macromolecules* **1993**, *26*, 561−562.
(10) Reiter, G. *Macromolecules* **1994**, *27*, 3046−3052.
(11) Doruker, P.; Mattice, W. L. *J. Phys. Chem. B* **1999**, *103*, 173−178.
(12) de Gennes, P. G. *Eur. Phys. J. E* **2000**, *2*, 201−205.
(13) Brown, S.; Szamel, G. *J. Chem. Phys.* **1998**, *109*, 6184−6192.
(14) Müller, M.; Wittmer, J. P.; Cates, M. E. *Phys. Rev. E* **1996**, *53*, 5063−5074.
(15) Tead, S. F.; Kramer, E. J.; Hadziioannou, G.; Antonetti, M.; Sillescu, H.; Lutz, P.; Strazielle, C. *Macromolecules* **1992**, *25*, 3642−3977.
(16) Ediger, M. D. *Annu. Rev. Phys. Chem.* **2000**, *51*, 99−128.
(17) Lax, M.; Brender, K. *J. Chem. Phys.* **1977**, *67*, 1785−1787.
(18) Metropolis, N.; Rosenbluth, A. W.; Rosenbluth, M. N.; Teller, A. H.; Teller, E. *J. Chem. Phys.* **1953**, *21*, 1087−1092.
(19) Mandel, F. *J. Chem. Phys.* **1979**, *70*, 3984−3988.
(20) Siepmann, J. I.; Frenkel, D. *Mol. Phys.* **1992**, *75*, 59−70.
(21) de Pablo, J. J.; Laso, M.; Suter, U. W. *J. Chem. Phys.* **1992**, *96*, 2395−2403.
(22) Dijsktra, M.; Frenkel, D.; Hansen, J. P. *J. Chem. Phys.* **1994**, *101*, 3179−3189.
(23) Mansfield, K. F.; Theodorou, D. N. *Macromolecules* **1989**, *22*, 3143−3152.
(24) Molina, L. A.; Freire, J. J. *Macromolecules* **1999**, *32*, 499−505.
(25) Clancy, T. C.; Mattice, W. L. *J. Chem. Phys.* **2000**, *112*, 10049−10055.
(26) Doi, M.; Edwards, S. F. *The Theory of Polymer Dynamics;* Oxford: New York, 1987; p 21.
(27) Kremer, K.; Grest, G. S. *J. Chem. Phys.* **1993**, *92*, 5057−5086.
(28) Donati, C.; Douglas, J. F.; Kob, W.; Plimpton, S. J.; Poole, P. H.; Glotzer, S. C. *Phys. Rev. Lett.* **1998**, *80*, 2338−2341.
(29) Khare, R.; de Pablo, J. J.; Yethiraj, A. *Macromolecules* **1996**, *29*, 7910−7918.
(30) Wignall, G. D. In *Encyclopedia of Polymer Science and Engineering*, 2nd ed.; Mark, H. F., Bikales, N. M., Overberger, C. C., Meneges, G., Eds.; Wiley-Interscience: New York, 1985; Vol. 10, p 112.
(31) Jones, R. L.; Kumar, S. K.; Ho, D. L.; Briber, R. M.; Russell, T. P. *Macromolecules* **2001**, *34*, 559−567.
(32) Angell, C. A. *Polymer* **1997**, *38*, 6261−6266.

MA011820E